Single-blind test of airplane-based hyperspectral methane detection via controlled releases

Evan D. Sherwin[1,†], **Yuanlei Chen**[1], **Arvind P. Ravikumar**[2] **and Adam R. Brandt**[1]

[1]Energy Resources Engineering, Stanford University, Stanford, California, United States of America
[2]Department of Systems Engineering, Harrisburg University of Science and Technology, Harrisburg, Pennsylvania, United States of America

E-mail: evands@stanford.edu

Abstract. Methane leakage from point sources in the oil and gas industry is a major contributor to global greenhouse gas emissions. The vast majority of such emissions come from a small fraction of "super-emitting" sources which, once detected, can generally be fixed at relatively low cost. We evaluate the emission detection and quantification capabilities of Kairos Aerospace's airplane-based hyperspectral imaging methane emission detection system. In blinded controlled releases of methane conducted over four days in San Joaquin County, California, USA, Kairos detected 182 of 200 valid nonzero releases, including all 173 over 8 mcfd(CH_4) per mile per hour (mph) of wind and none of the 8 nonzero releases below 4 mcfd(CH_4)/mph. There were no false positives: Kairos did not detect methane during any of the 19 negative controls. Plume quantification accuracy depends on the wind measurement technique, with a parity slope of 1.15 (σ=0.037, R^2=0.84, N=185) using a cup-based wind meter and 1.45 (σ=0.059, R^2=0.80, N=157) using an ultrasonic anemometer. Quantification error scales roughly as a fixed percentage of emission size. These findings suggest that at 5 mph winds under favorable environmental conditions in the US, Kairos could detect over 50% of total emissions by identifying super-emitting sources.

1. Introduction

US natural gas (NG) production reached 110 billion cubic feet per day (bcfd) in August 2019, a 56% increase over the past decade [1]. The shift from coal toward less-carbon-intensive NG and renewables have reduced the carbon intensity of the US power sector [2]. However, the climate benefits of NG cannot be fully realized if methane leaks into the atmosphere at significant rates, as methane has a global warming potential that is 28-36 times that of carbon dioxide over a 100-year period [3].

The US Environmental Protection Agency (EPA) greenhouse gas inventory states that NG and petroleum systems accounted for 32% of total US methane emissions and about 4% of total US greenhouse gas emissions in 2017 [4]. Field surveys in gas-producing regions suggest that the EPA inventory underestimates NG methane emissions, likely because EPA's process-based approach does not sufficiently account for emissions from extremely large sources [5–7]. Emission sizes in the North American NG supply chain are found to follow a heavy-tailed distribution, where the top 5% of the point sources (the so-called "super-emitters") contribute over 50% of total emissions [5]. A recent study indicates that 10% of the methane point sources in California (including oil and gas facilities, landfills, wastewater treatment plants, and dairy manure management sites) are responsible for 60% of

the detected point-source emissions [8]. Therefore, leak detection and repair (LDAR) programs could reduce the cost of detection and mitigation by allowing mitigation efforts to focus on the largest sources. Given the limited resources and manpower available for detection and repair, technologies for rapidly and accurately identifying super-emitters are essential for guiding mitigation efforts.

Close-range approaches, such as Method-21 and optical gas imaging, are widely employed in ground-based LDAR programs in the oil and gas industry. These methods are effective for source identification [9], but can be slow and labor-intensive. Mobile systems with sensors placed on trucks, drones, or aircraft have the potential advantage of speeding up detection by avoiding the need for manual detection via in-person site visits [10]. In particular, mobile remote sensing via airplanes or satellites can be used to target super-emitters, providing benefits of "low per-site cost, high spatial coverage, and frequent sampling" [11].

We examine a system developed by Kairos Aerospace (henceforth "Kairos"). Kairos' LeakSurveyor^{TM} is a hyperspectral methane imaging system that is mounted on a light aircraft flown at general aviation altitudes of approximately 900 m (3,000 feet) above ground level. The system uses an infrared imaging spectrometer to detect methane, an optical camera to create an optical surface map of the surveyed region, and GPS and inertial measurement units to record the position and orientation of the sensor [12]. LeakSurveyor^{TM} is capable of surveying 150 square miles of oil and gas infrastructure in a single day [12]. Figure 1(a) shows an example of a detected plume superimposed on an optical image of the ground below the airplane. See Supplementary Information (SI) section S1 for more details of the Kairos technology.

This study performs large-volume single-blind controlled releases. Figures 1(b) and 1(c) show the release equipment used. This study is motivated in part by the Mobile Monitoring Challenge (MMC), organized by the Stanford Natural Gas Initiative and the Environmental Defense Fund (EDF). The 2018 MMC tested ten methane detection technologies through single-blind controlled releases, with 6 out of the 10 participating technologies "correctly detecting over 90% of test scenarios (true positive plus true negative rates)" [10].

In contrast, we focus on characterizing quantification accuracy of the super-emitting methane point sources that LeakSurveyor was designed to quickly identify through aerial surveys. As a result, our emission rates are three to four orders of magnitude larger than those in the MMC, reaching 1,800 mcfd, as opposed to 0.36 mcfd for most near-ground technologies in the MMC and 36 mcfd for two airplane and truck-based technologies [10].

2. Methods

2.1. Airplane-based methane sensing technology

Kairos' methane detection technology uses hyperspectral imaging from the wing of a small aircraft to construct a two-dimensional image of methane concentrations integrated along the path between the airplane and the ground. Each image is generated through a single pass over a ground area. Kairos' automated processing identifies methane plumes and calculates wind-adjusted methane emission rate in thousands of standard cubic feet of methane per day per mile per hour of wind (mcfd(CH_4)/mph, henceforth denoted mcfd/mph). Note that the spectrometer detects only methane and not other constituent components of natural gas, such as ethane. See SI section S1 for further technical detail.

2.2. Test location and set-up

The Stanford team performed four days (October 8th, 10th, 11th, and 15th, 2019) of single-blind controlled releases on an airstrip in San Joaquin County, California. Figure 1(a) is an aerial image taken by Kairos and indicates the locations of the test devices. Kairos personnel were in the aircraft but were not present at the ground release site. Stanford personnel designed the release schedule and controlled the release rates with assistance from a natural gas release operator, Rawhide Leasing.

Figure 1 shows the release apparatus connecting compressed natural gas (CNG) trailers to three ∼2 m (6 feet) vertical release stacks, 2.5 cm (1 inch) in diameter. Each release stack is connected to gas equipment via a rubber hose 45.7 m (150 feet) in length.

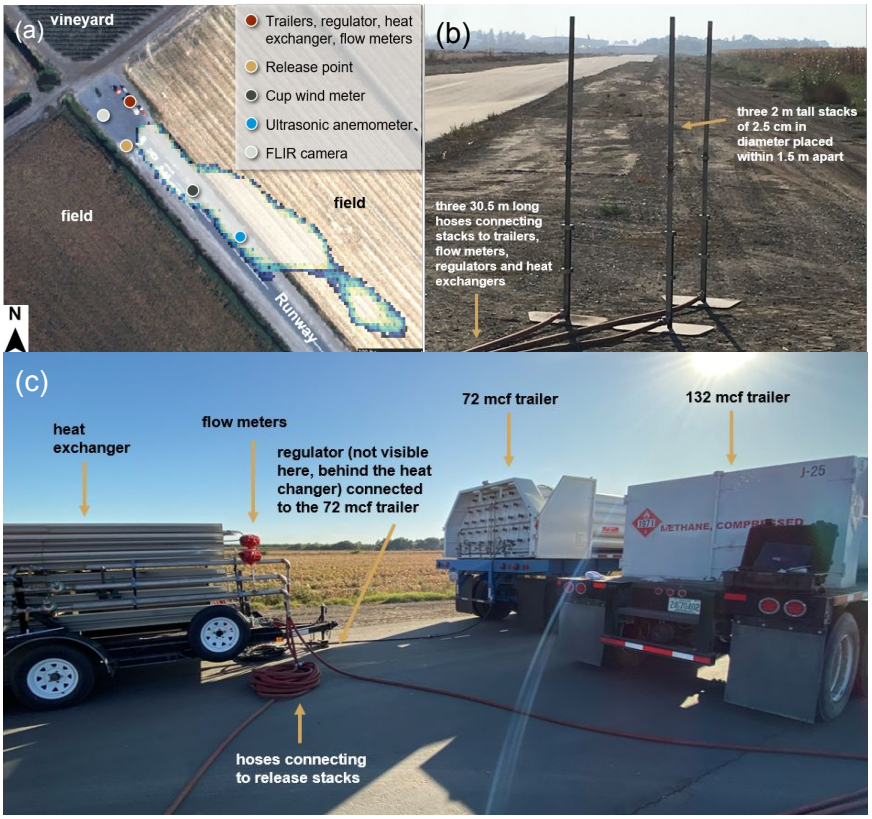

Figure 1. (a) Georeferenced image of a methane plume superimposed on an optical image taken by LeakSurveyor^{TM}, with locations of truck and trailers, release point, and anemometer annotated. This image is generated using Kairos technology. (b) Releasing stacks and hoses set up at the brown dot in (a). (c) Configuration of trailers, regulator, heat exchanger, flow meters, and hoses.

Figure 1(b) shows the three release stacks were placed together (1-1.5 m apart). This design allows larger release volumes. When methane simultaneously flows from the three stacks, the gas released forms a single plume due to rapid mixing below the boundary layer of the atmosphere. Infrared images of the plumes from a FLIR infrared camera confirm that plumes rapidly mix and equilibrate in temperature. see SI section S3 for further detail.

Two trailers of CNG (93.5 vol% methane, 5.0 vol% ethane, 1.5 vol% trace gases) were transported to the site by Rawhide Leasing and placed at the red dot in Figure 1(a) [13]. This location was generally upwind of the release point. The two trailers, with capacity of 72 mcf and 132 mcf, respectively, are

henceforth referred to as "small trailer" and "big trailer". Because the detector measures only methane, all release gas rates are reported in units of methane, scaling the measured gas release rate from the meter by 0.935.

Natural gas released from the small trailer first travels through a regulator and a heat exchanger. The regulator steps down the pressure of CNG from a maximum of 172 bar (2,500 psi) in the tank to less than 34 bar (500 psi) before releasing. To compensate for the Joule-Thomson cooling effect, the gas passes through a heat exchanger to bring gas to approximately ambient temperature [14]. The big trailer is configured with a different regulator for flow control but was not attached to a heat exchanger. At high release rates, methane from the regulator without a heat exchanger reached temperatures as low as as $-45°C$ $(-50°F)$ at the flow meter and the hose developed frost, shown in Figure S2. However, as the cold gas reached the atmosphere, it quickly equilibrated to roughly atmospheric temperature, as shown in an infrared camera image in SI section S3, showing a minimum temperature of $18.4°C$ $(65°F)$ at the release point.

After pressure and temperature regulation and before entering rubber hoses that carried the gas to the release stacks, the three streams of gas were individually metered with Sierra Instruments QuadraTherm 740i thermal mass flow meters. These meters have rated accuracy of $\pm 0.5\%$ of reading above 50% of full scale (calibrated to 30,700 scfd of natural gas volume, not methane volume) and $\pm 0.5\%$ of reading plus $\pm$0.5% of full scale if reading is below 50% of full scale flow [15]. The meter error associated with the methane flow rate is taken to be 93.5% of the rated flow meter accuracy, converting from natural gas volume to methane volume.

The image of the plume is used to estimate the emissions rate using a mass-balance approach across a central section of the plume. This approach relies on advection of methane downwind in the dominant wind direction, while the plume spreads in the transverse directions. Thus, the reported emission rates are rates normalized to wind speed, i.e., in mcf of methane per day per mph of wind (mcfd/mph). The wind speed (ideally measured near the release point) is then used to convert this estimate to an absolute emissions rate (mcfd).

We measured wind speed and direction using both a Vantage Vue Sensor Suite with a cup-based wind meter and a Gill Instruments WindSonic 60 two-dimensional ultrasonic anemometer. The cup wind meter measures wind speed with a resolution of $\sim$0.5 m/s (1 mph) and an accuracy of ± 1 m/s (± 2 mph) every 2.5 seconds. Data are logged every minute to output 1-minute average wind speed and 1-minute gust (maximum) wind speed [16].

We used the ultrasonic anemometer on the final three days of data collection (Oct 10, 11, 15th). This anemometer measures wind speed with a resolution of 0.01 m/s and accuracy of $\pm 2\%$ at 12 m/s [17]. The ultrasonic anemometer logs data every second. We then compute 1-minute average and 1-minute gust wind speed. We mounted both wind meters on 2.5-m (8-foot) meteorological tripods. Due to the partial absence of wind data from the ultrasonic anemometer during the controlled release, we use the wind data from the cup wind meter in the base case. See the SI, Section S6 for a comparison of the two wind meters.

The daily flight time window was between 9:45am and 4:00pm due to the need for sufficient illumination. Heavy cloud cover can interfere with the performance of Kairos' instrument. We cancelled data collection on October 9 due to the predicted presence of such clouds.

In addition, high wind speeds can render conditions unsafe for the small airplane currently used

to deploy Kairos' instrument. On October 10th, we conducted the tests only in the afternoon because morning gust wind speed was over 15 mph, which was considered unsafe for flights. It may be possible to deploy the instrument at higher wind speeds using a larger or more wind-robust airborne deployment mechanism.

2.3. Single-blind experimental design

The aerial test used a two-person airplane with Kairos' LeakSurveyor^{TM} instrument fastened to one wing strut, occupied by one pilot and one Kairos engineer. The Kairos engineer oversaw operations and radio communication with ground crews from Stanford and Rawhide. Kairos' instrument was mounted on the plane and took images of the methane plume when the aircraft passed over the test site. The aircraft flew repeated North-South round-trip passes on a fixed route, passing overhead roughly every four minutes, varying from three to five minutes depending on wind and other environmental conditions.

Aircraft overflights were logged by both the Stanford and Kairos teams. Roughly 30 seconds before the plane passed over the test site, the Kairos engineer informed the Stanford ground crew of the upcoming flight pass via a two-way radio connection. When the Stanford ground crew visually determined the airplane was overhead, we recorded the release rates indicated by all active flow meters, also noting the precise time and instantaneous wind conditions from the cup-based wind meter. Wind data used for analysis are drawn from digital logs produced by the cup wind meter and ultrasonic anemometer at the pass timestamps recorded by the Stanford ground crew. The Kairos engineer in the airplane independently recorded timestamps when the airplane passed overhead.

During the single-blind controlled releases, only Stanford personnel and one operator from Rawhide Leasing were aware of the release schedules and the actual release rates and ground-based wind measurements. Rawhide personnel did not have access to radio transceivers and did not write down any flow rates. It should be noted that Kairos had knowledge of the size of the trailers during the single-blind tests. However, this awareness of the upper bound on total daily releases has little potential of breaking the blind because the daily average release rate was always well below the level required to exhaust all on-site tank capacity. Kairos reported final results to Stanford on October 24th and Kairos received actual release rates and ground-based wind measurements on October 29th.

2.4. Sampling strategy

We outlined the release schedule in advance and adapted in real time in response to changing environmental conditions and a continuously improving understanding of the capabilities of the equipment.

On average, the Stanford team changed the release rate every seven flight passes, roughly every 30 minutes. The procedure was randomized with a minimum constant release level duration of one pass and a maximum of 27 passes to reduce the potential possibility of Kairos guessing of release rates based on previous measurements. Wind speed varied significantly across flight passes (see SI section S7 for detailed wind speed measurements) and Kairos did not have access to ground measurements of wind speed prior to reporting their quantification results. Fluctuations in the measured mass flow rate are on the order of flow meter uncertainty. See the SI, Section S8 for further detail.

2.5. Performance metrics

We test Kairos' technology for detection accuracy, minimum detection threshold, and quantification accuracy. Here, detection accuracy is defined as the sum of true positive and true negative rates. The minimum detection threshold analysis characterizes both the minimum release rate that the technology can detect with some nonzero probability and the rate above which all releases are detected. Quantification accuracy compares the estimated methane release rates to the true release rate.

2.6. Data exclusion criteria

We exclude data points based on the following criteria. See SI section S4 for a detailed description of these exclusion criteria and alternative exclusion criteria.

(i) Incorrect airplane altitude

(ii) Insufficient time for plume development

(iii) Multiple methane release points (abandoned after the first day of trials)

(iv) Wind speeds below the rated uncertainty range of the wind meter

(v) Plume image cut off from field of view, thus preventing accurate quantification

3. Results

3.1. Data summary

A total of 230 data points were collected during the four-day single-blind tests, among which 21 ($\sim$10%) were negative controls during which no methane was released. 37 releases ($\sim$15%) were designed to find the detection threshold by releasing at a rate between 0-50 mcfd. The remaining large releases ($\sim$75% of releases) were focused on testing the ability of the system to quantify release volumes. Among these, 57 releases were within the range of 50 and 500 mcfd; and 116 were over 500 mcfd. The above-mentioned flow were measured by the flow meters. Note that methane flow rates are 93.5% of metered natural gas flow rates [13].

Of the 230 data points collected, 9 are excluded from the baseline analysis due to technical issues such as incomplete image of plume captured and controlled release practices that deviated from protocol. 4 additional data points were not collected due to an incorrect flight altitude (see SI section S2 for details). Kairos detected 182 of 200 valid nonzero releases. An additional 8 data points associated with cup-wind-meter-measured wind speed less than or equal to 2 mph ($\sim$1 m/s) are excluded from the quantification accuracy analysis, because these trials have wind-related error bars that cross zero due to uncertainty in wind measurements, rather than uncertainty in Kairos' plume quantification.

Data points are also excluded from the quantification analysis if there is not sufficient time after a change in release level for full development. We waited 30 seconds after each overflight before any change in the release rate to ensure clean measurements. Changing release rates generally took roughly 30 seconds. So, given the average four-minute interval between observations, a plume has roughly three minutes to stabilize between overflights after a change in the release rate. Thus, we include only data points for which a gas particle traveling at the 1-minute gust wind speed would traverse the full length of the plume between a change in release levels and the observation, three minutes. It generally took

another 30 seconds for the flow to stabilize at a new level, leaving three minutes out of the 4-minute test interval for the new plume to fully develop. We exclude 8 data points due to insufficient time for plume development.

After applying all exclusion criteria, we present data from 205 single-blind releases in the results section, of which 185 data points involve gas release (the rest are negative controls). We present results using alternative data exclusion criteria in SI section S5.

Figure 2 shows images of methane plumes detected by the Kairos instrument during the trial. Plume images are colorized, with blue representing low concentrations of methane and white representing high concentrations. All connected pixels are considered to be within a single plume. If there are multiple disconnected plumes, we analyze the closest plume to the release point by the end of the airstrip, consistent with Kairos' internal practices. Figure 2a shows a Kairos image while no methane is being released. Figure 2b shows a small plume over the airstrip at a wind-adjusted release rate of 7.2 mcfd/mph, approaching the minimum detection threshold of the instrument. The plume in Figure 2c is clearly visible, with a wind-adjusted release rate of 38.7 mcfd/mph. Figures 2d-f show larger plumes with a wider field of view. Note small patches of blowoff methane, separated from the main plume, in Figures 2d and 2e, and the tenuously-connected shape of the large plume in Figure 2f, indicating variability in the wind direction.

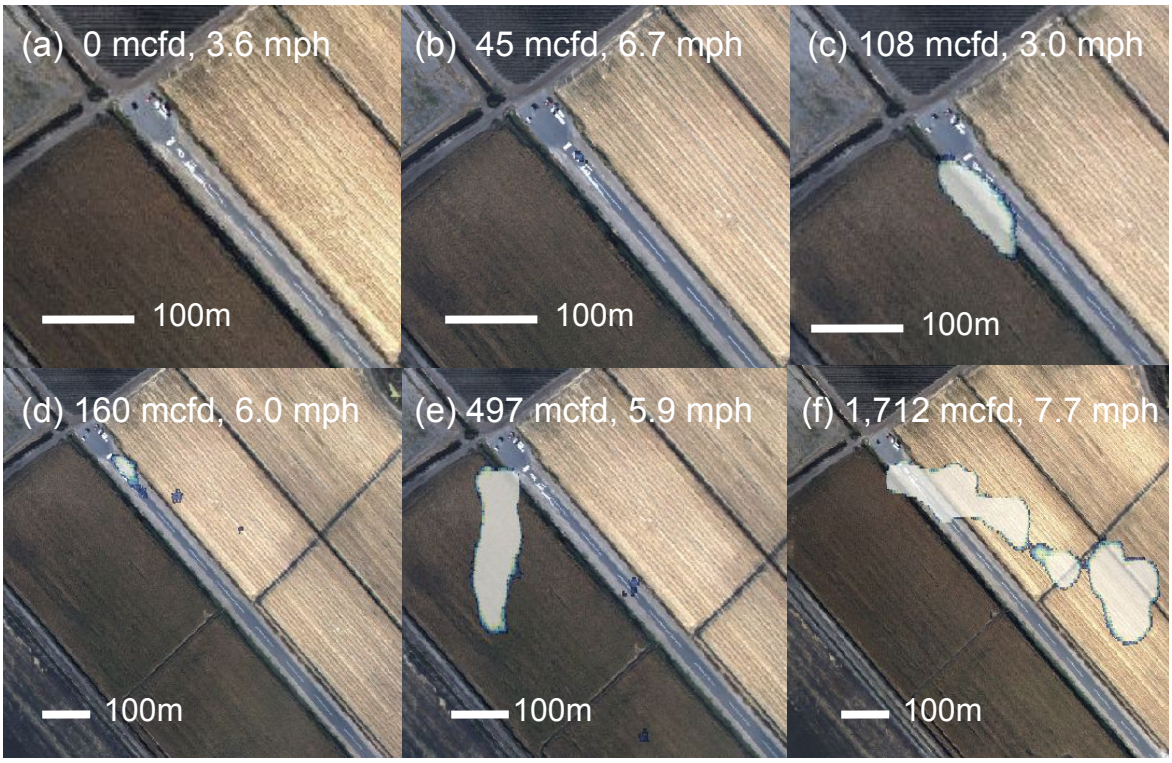

Figure 2. Examples of detected plumes associated with different release rates. Plumes are shown in colorized spectrometer images, with blue and white representing low and high concentrations of methane, respectively. Optical images were taken from the airplane as the airplane was overhead. Each image includes the measured methane release rate, in mcfd, and wind speed from the ultrasonic anemometer. Note that the scale changes in the bottom row, d-f. (a) No release. (b) Small release, close to detection threshold. (c) Medium-sized release, low wind. (d) Medium-sized release, moderate wind. (e) Large emission, moderate wind. (f) Approaching maximum release rate, moderate wind.

3.2. Detection probability and false positive rate

Kairos previously published work reporting a 50% probability of detection at 5.5 mcfd/mph [12]. Considering the limited resources available for this study and the interest in testing quantification accuracy at large emission rates, only 15% of data points have nonzero release rates <50 mcfd. Due to exclusion criteria and the wind speed conditions at the time of the release, 36 valid data points fall in the range of 0-12 mcfd/mph and are presented in Figure 3.

Figure 3 shows the fraction of emissions detected by the Kairos technology as a function of wind-speed-normalized methane release rate. Below 4 mcfd/mph, the instrument detected none of the eight nonzero emissions. The detection rate rises to 33% for release rates of 4-6 mcfd/mph, rising to 71% for release rates from 6-8 mcfd/mph. Above 8 mcfd/mph, 100% of emissions were detected (9/9). Thus, we expect that 50% probability of detection will occur in the range of 4-8 mcfd/mph, consistent with Kairos' internal trials. Error bars represent two standard deviations assuming a binomial distribution, with no error bars shown for cases with 100% or 0% detection rates. This suggests that the instrument can detect all emissions above about 8 mcfd/mph with high probability.

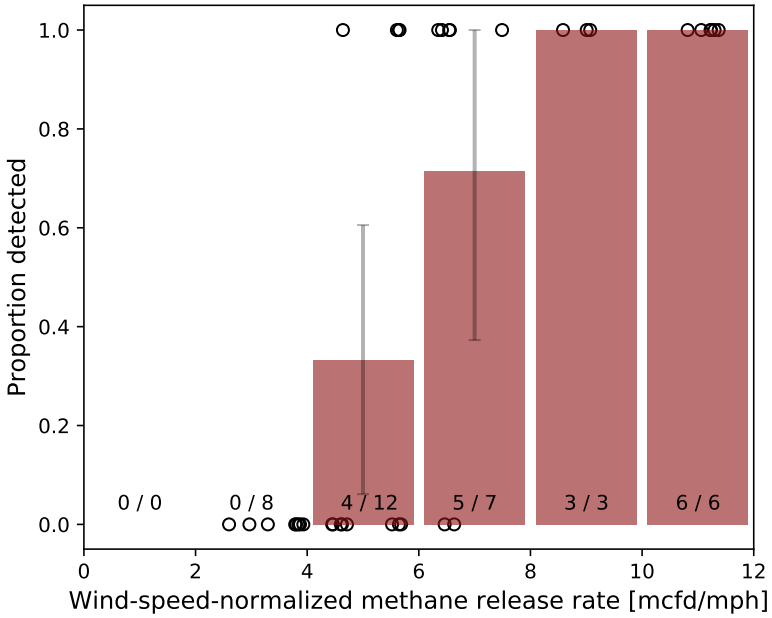

Figure 3. Binary detection results and the proportion of releases detected when the true release rates fall in the range of 0-12 mcfd/mph. Each bin has a width of 2 mcfd/mph. Error bars show two standard deviations assuming a binomial distribution. The numbers of true positives / the numbers of releases conducted are annotated at the bottom of the bins.

To test for false positives, we set ∼10% of release segments (24 segments) to release rates of 0 mcfd. Kairos reported no detections during these segments, leading to a false positive rate of 0%. This is in part because such remote sensing techniques are less sensitive than many other methane detectors and require larger signal to register detection, missing small emissions but rarely triggering false positives. Thus, Kairos detected all 173 releases over 8 mcfd per mile per hour (mph) of wind and none of the 8

nonzero releases below 4 mcfd/mph.

3.3. Quantification accuracy

Figure 4(a) shows 185 valid data points associated with nonzero release rates, comparing the meter-measured release rates (x-axis) to the estimated rates generated by Kairos. The estimated releases in mcfd are computed as Kairos-reported number in mcfd/mph multiplied by 1-min gust wind speed in mph (measured with cup-based wind meter) at the time of each pass. Kairos' technology produces point estimates with no uncertainty in mcfd/mph. Uncertainties in wind measurements are ± 2 mph and the resulting errors in the reported release rate due to uncertainties in wind are shown in Figure 4(a). The length of the error bars are thus dependent on the magnitude of the Kairos-reported number in mcfd/mph. The y-axis of Figure 4(b) shows the Kairos-reported number multiplied by 1-min gust wind speed measured with ultrasonic anemometer, which has a rated accuracy of $\pm 2\%$ at a wind speed of 12 m/s ($\sim$27 mph) [17]. We assume that this holds for all wind speeds. In this case, the length of the error bars depends both on the magnitude of the measured wind speed and the Kairos-reported quantification in mcfd/mph.

Wind measurement uncertainties substantially exceed the magnitudes of wind variability and known release rate variability. Therefore, the two latter variabilities are not included in Figure 4. A comparison of wind data collected by the two devices and more discussion on wind and release rate variability are available in the SI, sections S6 and S8. The ultrasonic anemometer had a much smaller measurement uncertainty but was only present for n = 157 releases. Therefore, results from cup wind meter measurements shown in Figure 4(a) are treated as a base case scenario for analysis.

The R^2 of the parity chart in Figure 4(a) is 0.84. The best fit regression line has a slope of 1.15 ($\sigma = 0.037$). 95% confidence intervals of the regression fit in Figure 4 are derived, with their lower bounds lying above the parity line, indicating an upward bias. However, note that the confidence intervals in Figure 4 assume homoskedasticity, which residual plots in Figure 5 suggest does not hold. Heteroskedastic confidence intervals would widen at higher release rates. Using ultrasonic anemometer wind data, R^2 drops to 0.80 and the best fit line exhibits a larger slope of 1.45 ($\sigma = 0.059$), indicating somewhat more bias at larger release rates.

Residual plots in Figure 5(a-b) exhibit heteroskedasticity. The percent residuals in Figure 5(c-d) show that the (observed - expected)/expected values do not change appreciably with increases in rate, showing a proportional growth in residual magnitude with the release size. Points clustered at -100% in Figure 5(c-d) are the false negatives with release rates below the minimum detection threshold.

3.4. Estimate of field efficacy

Using a bottom-up inventory of 1009 methane emission sites from the US oil and gas system from Omara et al. 2018 [18], we estimate that given 5 mph winds and emission detection fractions based on the probabilities from Figure 3, adoption of this technology would detect 53% of total emissions, with 49% coming from 30 sites above the 100% detection threshold of 8 mcfd/mph. At 3 mph winds, this rises to 61% of total emissions. At 10 mph winds, this falls to 41% of total emissions. Note that this inventory combines emissions from multiple basins. In practice, detector efficacy would likely vary across basins due to different emission profiles. In addition, we do not perform a full stochastic techno-economic

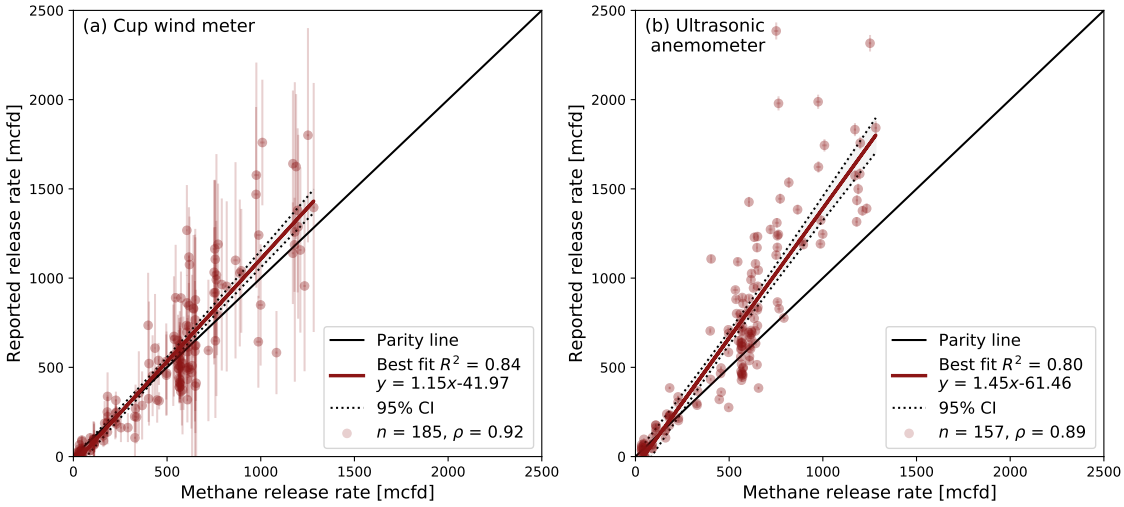

Figure 4. Parity chart of known nonzero methane release rates and Kairos reported release in mcfd/mph multiplied with 1-min gust wind speed in mph measured by (a) cup wind meter and (b) ultrasonic anemometer. The X=Y parity line indicates perfect quantification. Y-error bars are uncertainties in wind measurements multiplied with wind-speed normalized release rate reported by Kairos. 95% confidence intervals of the regression fits are shown. n = number of data points shown in each graph.

analysis, such as that in the Fugitive Emissions Abatement Simulation Toolkit, which would be necessary to determine the cost-effective mitigation potential of airplane-based methane sensing technology [19].

4. Conclusions

We examine the efficacy of Kairos technology at detecting and quantifying methane emissions at moderate to large release rates, with an emphasis on verifying quantification performance for large emissions. Results from controlled releases show that Kairos' technology was able to detect 100% of emissions above 8 mcfd/mph. No emission below 4 mcfd/mph was detected. Kairos had false positive rate of 0%: zero-emission conditions were never erroneously identified as nonzero emissions. The technology was able to quantify methane emissions with an R^2 of $\sim$0.8, suggesting a relatively close linear fit with random error scaling roughly as a fixed percentage of the estimated emission rate.

Aerial surveys at modest wind speeds could detect 50% or more of total methane emissions at substantially lower cost than traditional leak detection and repair methods. Thus, this technology could provide rapid detection of super-emitting methane leaks, likely as a supplement to more precise but more labor-intensive leak detection and repair programs.

Acknowledgement

This study was funded by the Stanford Natural Gas Initiative, an industry consortium that funds independent research at Stanford University. No funding was provided by participating or tested companies. The authors would like to thank Jingfan Wang, Jeffrey Rutherford, and Alison Marsden at

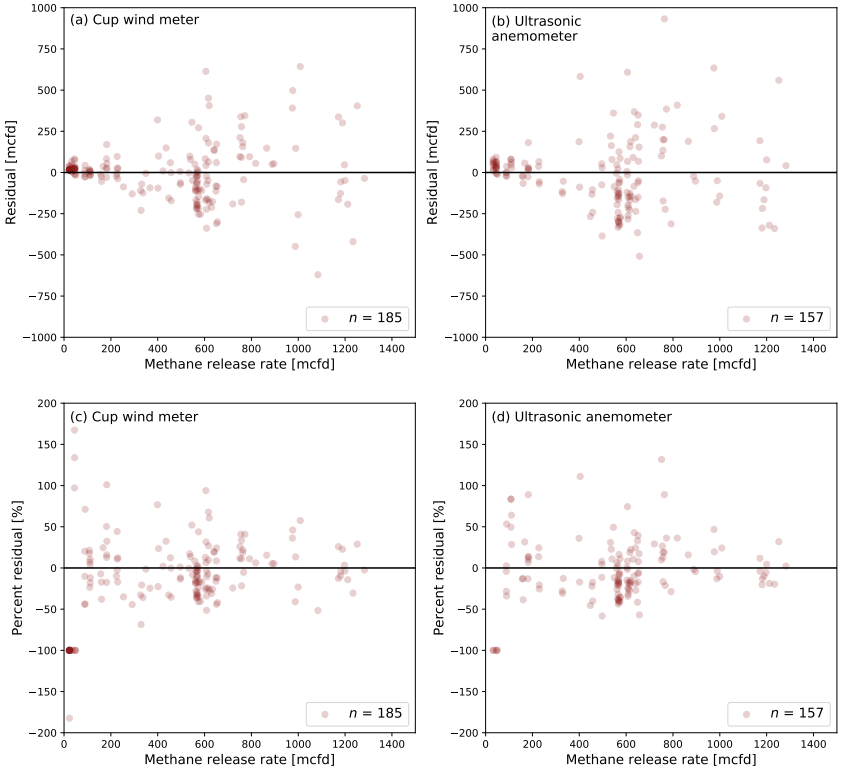

Figure 5. (a-b) Regression residuals and (c-d) percent residuals from regression predictions as a function of known methane release rates. Note that the distribution of percent residuals is approximately uniform in methane release rate, suggesting that quantification error is approximately constant as a percentage of the measured value.

Stanford, and Jeff Gamble and Walter Godsil from Rawhide Leasing for help with the controlled release, as well as Chris Field, Jennifer Johnson, Keith Andre, and Jon Carlson for their support with wind measurements. We gratefully acknowledge the assistance of Tony Ramirez and the staff of Zuckerman Family Farms.

References

[1] EIA. Monthly Crude Oil and Natural Gas Production. Technical Report EIA-914, U.S. Energy Information Administration, Washington, D.C., November 2019.

[2] Power Sector Carbon Index. Technical report, Carnegie Mellon University Scott Institute for Energy Innovation, Pittsburgh, PA, USA, 2019.

[3] EPA. Greenhouse Gas Emissions: Understanding Global Warming Potentials. Technical report, US Environmental Protection Agency, February 2017.

[4] US EPA. Inventory of U.S. Greenhouse Gas Emissions and Sinks: 1990-2017. Technical Report EPA430-R-19-001, United States Environmental Protection Agency, Washington, D.C., April 2019.

[5] A. R. Brandt, G. A. Heath, E. A. Kort, F. O'Sullivan, G. Petron, S. M. Jordaan, P. Tans, J. Wilcox, A. M. Gopstein, D. Arent, S. Wofsy, N. J. Brown, R. Bradley, G. D. Stucky, D. Eardley, and R. Harriss. Methane Leaks from North American Natural Gas Systems. *Science*, 343(6172):733–735, February 2014.

[6] David R. Lyon, Ramn A. Alvarez, Daniel Zavala-Araiza, Adam R. Brandt, Robert B. Jackson, and Steven P. Hamburg. Aerial Surveys of Elevated Hydrocarbon Emissions from Oil and Gas Production Sites. *Environmental Science & Technology*, 50(9):4877–4886, May 2016.

[7] Daniel Zavala-Araiza, David R. Lyon, Ramn A. Alvarez, Kenneth J. Davis, Robert Harriss, Scott C. Herndon, Anna Karion, Eric Adam Kort, Brian K. Lamb, Xin Lan, Anthony J. Marchese, Stephen W. Pacala, Allen L. Robinson, Paul B. Shepson, Colm Sweeney, Robert Talbot, Amy Townsend-Small, Tara I. Yacovitch, Daniel J. Zimmerle, and Steven P. Hamburg. Reconciling divergent estimates of oil and gas methane emissions. *Proceedings of the National Academy of Sciences*, page 201522126, December 2015.

[8] Riley M. Duren, Andrew K. Thorpe, Kelsey T. Foster, Talha Rafiq, Francesca M. Hopkins, Vineet Yadav, Brian D. Bue, David R. Thompson, Stephen Conley, Nadia K. Colombi, Christian Frankenberg, Ian B. McCubbin, Michael L. Eastwood, Matthias Falk, Jorn D. Herner, Bart E. Croes, Robert O. Green, and Charles E. Miller. California's methane super-emitters. *Nature*, 575(7781):180–184, November 2019.

[9] Arvind P. Ravikumar, Jingfan Wang, Mike McGuire, Clay S. Bell, Daniel Zimmerle, and Adam R. Brandt. "Good versus Good Enough?" Empirical Tests of Methane Leak Detection Sensitivity of a Commercial Infrared Camera. *Environmental Science & Technology*, 52(4):2368–2374, February 2018.

[10] Arvind P Ravikumar, Sindhu Sreedhara, Jingfan Wang, Jacob Englander, Daniel Roda-Stuart, Clay Bell, Daniel Zimmerle, David Lyon, Isabel Mogstad, Ben Ratner, and Adam R Brandt. Single-blind Inter-comparison of Methane Detection Technologies - Results from the Stanford/EDF Mobile Monitoring Challenge. *Elementa: Science of the Anthropocene*, 7(37):29, September 2019.

[11] Thomas A Fox, Thomas E Barchyn, David Risk, Arvind P Ravikumar, and Chris H Hugenholtz. A review of close-range and screening technologies for mitigating fugitive methane emissions in upstream oil and gas. *Environmental Research Letters*, 14(5):053002, April 2019.

[12] Kairos. Kairos Aerospace Technical White Paper: Methane Detection. Technical report, Kairos Aerospace, Mountain View, CA, USA, 2019.

[13] PG&E. California Gas Transmission | Pipe Ranger | Operating Data | Gas Quality. Technical report, Pacific Gas and Electric Co., San Francisco, CA, USA, 2019.

[14] S. Angus, B. Armstrong, and K.M. de Reuck. Chapter 5. Methane. In *International thermodynamic tables of the fluid state*. United States, January 1978.

[15] Sierra. Sierra: QuadraTherm 780i. Technical report, Sierra Instruments, 2019.

[16] Vantage Vue Weather Station. Technical report, Davis Instruments, Hayward, CA, USA, December 2018.

[17] Gill. Wind Speed & Direction Sensor. Technical report, Gill Instruments, Lymington, Hampshire, UK, 2019.

[18] Mark Omara, Naomi Zimmerman, Melissa R. Sullivan, Xiang Li, Aja Ellis, Rebecca Cesa, R. Subramanian, Albert A. Presto, and Allen L. Robinson. Methane Emissions from Natural Gas Production Sites in the United States: Data Synthesis and National Estimate. *Environmental Science & Technology*, 52(21):12915–12925, November 2018.

[19] Chandler E. Kemp, Arvind P. Ravikumar, and Adam R. Brandt. Comparing Natural Gas Leakage Detection Technologies Using an Open-Source "Virtual Gas Field" Simulator. *Environmental Science & Technology*, 50(8):4546–4553, April 2016.